

# Gap Estimation by means of Hyperbolic Deformation

Hiroshi UEDA<sup>1</sup>, Hiroki NAKANO<sup>2</sup>, Koichi KUSAKABE<sup>1</sup>, and Tomotoshi NISHINO<sup>3</sup>

<sup>1)</sup> *Department of Material Engineering Science, Graduate School of Engineering Science, Osaka University, Osaka 560-8531*

<sup>2)</sup> *Graduate School of Material Science, University of Hyogo, Kouto 3-2-1, Kamiori, Ako-gun, 678-1297*

<sup>3)</sup> *Department of Physics, Graduate School of Science, Kobe University, Kobe 657-8501*

(Received November 17, 2018)

We present a way of numerical gap estimation applicable for one-dimensional infinite uniform quantum systems. Using the density matrix renormalization group method for a non-uniform Hamiltonian, which has deformed interaction strength of  $j$ -th bond proportional to  $\cosh \lambda j$ , the uniform Hamiltonian is analyzed as a limit of  $\lambda \rightarrow 0$ . As a consequence of the deformation, an excited quasi-particle is weakly bounded around the center of the system, and kept away from the system boundary. Therefore, insensitivity of an estimated excitation gap of the deformed system to the boundary allows us to have the bulk excitation gap  $\Delta(\lambda)$ , and shift in  $\Delta(\lambda)$  from  $\Delta(0)$  is nearly linear in  $\lambda$  when  $\lambda \ll 1$ . Efficiency of this estimation is demonstrated through application to the  $S = 1$  antiferromagnetic Heisenberg chain. Combining the above estimation and another one obtained from the technique of convergence acceleration for finite-size gaps estimated by numerical diagonalizations, we conclude that the Haldane gap is in  $[0.41047905, 0.41047931]$ .

**KEYWORDS:** DMRG, renormalization group, excitation gap, antiferromagnetic Heisenberg chain, Haldane gap, exact-diagonalization method

## 1. Introduction

Analysis of elementary excitations has been one of the central concerns in the condensed matter physics. The ground state of an infinitely large quantum system, that has a finite excitation gap, is quite different from the gapless systems in its correlation properties. Precise estimation of the excitation gap is therefore important, particularly in numerical analysis of correlated systems.

Because of limitation in computational resources, it is difficult to handle directly an infinite size system, but precise numerical analysis is possible on data for finite size systems. The method of finite size scaling (FSS) has been employed for the extrapolation of the data to the infinite size limit.<sup>1,2</sup>

As an example of the gapped system, let us consider a spin- $S$  antiferromagnetic Heisenberg chain. When  $S$  is an integer, the system has a nonzero excitation energy  $\Delta$ , which is known as the Haldane gap.<sup>3-5</sup> In estimation of this gap, finite size corrections should be subtracted properly from the numerical data. Reliability of such extrapolation procedure is partially dependent on the maximum of available system size that is handled by computation resources. In the case of the  $S = 1$  chain, the maximum at present is around 24 by use of the Lanczos diagonalization,<sup>6-8</sup> but it becomes thousands by use of the density matrix renormalization group (DMRG) method.<sup>9-12</sup>

Appropriate choice of the boundary condition is an important procedure for the precise estimation of the excitation gap. In case of a one-dimensional system with open boundary conditions, reflection at the system boundary occasionally gives a nontrivial contribution to the kinetic energy of the excited quasi particle, while the particle itinerates in the whole system. Such a reflection effect can be reduced by means of a fine tuning of the boundary

condition. In case of the  $S = 1$  chain, an efficient way is to put an additional  $S = 1/2$  spin at each end of the system, and to reduce the value of  $J_{\text{end}}$ , the coupling constant between the  $S = 1$  and the  $S = 1/2$  spins at the boundary, compared with  $J$ , the exchange interaction inside the system. The value  $\Delta = 0.41050(2)$  was reported under the condition  $J_{\text{end}} = 0.5088$ .<sup>13</sup> In order to obtain a precise reference data for the following study in this article, we swept the value of  $J_{\text{end}}$ , and obtained a slightly smaller value  $\Delta = 0.41047944(27)$  when  $J_{\text{end}} = 0.50866$ ,<sup>14</sup> as shown in this paper. It should be noted that this kind of fine tuning at the system boundary is necessary for each system under study. For example, if the  $S = 1$  chain contains uniaxial anisotropy, the most appropriate value of  $J_{\text{end}}$  is dependent on the anisotropy parameter.

In this article we propose a way of erasing the boundary reflection effect, by weakly confining the excited quasiparticle around the center of the system. For this purpose, we introduce the so-called hyperbolic deformation to the one-dimensional quantum Hamiltonians, where interaction strength between neighboring sites is proportional to  $\cosh \lambda j$ . Here,  $j$  is the lattice index running from  $-\infty$  to  $\infty$ , and  $\lambda$  is the deformation parameter.<sup>15</sup> Although the interaction strength becomes position dependent, the ground state preserves a uniform property for any positive  $\lambda$ . For example, the expectation value of the bond energy of the deformed Heisenberg chain is almost position independent. This uniform property in the ground state can be explained from the geometrical interpretation of the hyperbolic deformation.

The effect of non-uniformity in the deformed Hamiltonian appears in the elementary excitation. As we show in the following study on the deformed  $S = 1$  Heisenberg chain, an excited quasiparticle is weakly attracted to the center of the system, where the width of the bound state is proportional to  $1/\sqrt{\lambda}$ . The corresponding excitation

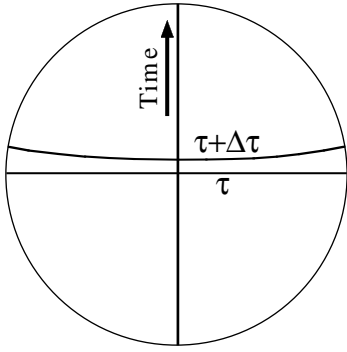


Fig. 1. Imaginary-time axis and equal-time lines in the hyperbolic plane drawn inside the Poincaré disc.

gap  $\Delta(\lambda)$  is nearly linear in  $\lambda$  when  $\lambda \ll 1$ . It is shown that the extrapolation of  $\Delta(\lambda)$  to the limit  $\lambda \rightarrow 0$  accurately gives the Haldane gap. The obtained value is compared with another value determined by the sequence interval squeeze (SIS) method.<sup>8</sup> The precise procedure of the SIS method developed by Nakano and Terai is explained in this article and another application of this method is given. This technique with the exact numerical diagonalization gives bounds for the Haldane gap. We will conclude definitely that the upper bound of the Haldane gap is given by  $\lim_{\lambda \rightarrow 0} \Delta(\lambda)$  much precisely than the SIS method. In this paper, the present best estimation of the lower bound given by the SIS method is also given.

In the next section we explain the geometric background of the hyperbolic deformation. As an example, we consider a deformed tight-binding model, and its continuum limit. In §3, we show the distribution of the magnetic quasiparticle under the deformation, where the observed shallow bound state is in accordance with the tight-binding picture. In §4, we perform extrapolation  $\lambda \rightarrow 0$  for the estimation of the excitation gap  $\lim_{\lambda \rightarrow 0} \Delta(\lambda)$ . As an independent estimate of the Haldane gap, we give the present best result by the SIS method in §5. Conclusions are summarized in the last section.

## 2. Hyperbolic Deformation

Real- or imaginary-time evolution of a one-dimensional (1D) quantum system is related to a 2D classical system through so called the quantum-classical correspondence.<sup>16–18</sup> Our aim here is to generalize the correspondence for a general case where the classical system is on curved 2D spaces. Let us consider a hyperbolic plane, which is a 2D space with constant negative curvature. Suppose that there is a uniform classical field on the hyperbolic plane, where the local action is position independent. Then, how does the corresponding 1D quantum Hamiltonian look like? We consider this problem for the case of imaginary-time evolution.

Figure 1 shows the 2D hyperbolic space drawn inside the Poincaré disc. All the geodesics are represented by arcs, which are perpendicular to the border circle, including straight lines that pass through the center of the disc. Let us regard the vertical line as the imaginary-time axis. Then all the geodesics that are perpendicular to

this imaginary-time axis can be regarded as equal-time curves. Suppose that the horizontal line corresponds to the coordinate  $x$  of the quantum system, and consider a quantum state  $|\Psi(\tau)\rangle$  on this line. If the classical action in the lower half of the hyperbolic plane is uniform, and if there is no symmetry breaking such as dimerization, the state  $|\Psi(\tau)\rangle$  is also translationally invariant. This is because  $|\Psi(\tau)\rangle$  is given by imaginary time boost from  $\tau = -\infty$ , which is mediated by the uniform action.

Let us consider an infinitesimal evolution

$$|\Psi(\tau + \Delta\tau)\rangle = \mathcal{U}[\Delta\tau] |\Psi(\tau)\rangle \quad (2.1)$$

from  $\tau$  to  $\tau + \Delta\tau$ , where  $\mathcal{U}[\Delta\tau]$  represents the imaginary-time boost operation. Though both  $|\Psi(\tau)\rangle$  and  $|\Psi(\tau + \Delta\tau)\rangle$  are translationally invariant,  $\mathcal{U}[\Delta\tau]$  is not. The fact can be seen geometrically by considering the distance between two points  $(x, \tau)$  and  $(x, \tau + \Delta\tau)$  on the hyperbolic plane, which is an increasing function of  $|x|$ . The distance can be represented as  $(\cosh \nu x) \Delta\tau$ ,<sup>19</sup> where  $\nu$  is a constant which is a function of the scalar curvature of the hyperbolic plane. If it is possible to represent  $\mathcal{U}[\Delta\tau]$  in the exponential form

$$\mathcal{U}[\Delta\tau] = \exp\left(-\int \hat{h}(x) (\cosh \nu x) \Delta\tau dx\right) = \exp(-\Delta\tau H), \quad (2.2)$$

the corresponding Hamiltonian  $H$  is also position dependent. In this case,  $H$  is written by an integral of a local operator  $\hat{h}(x)$ , and the position dependence is explicitly written as

$$H = \int (\cosh \nu x) \hat{h}(x) dx. \quad (2.3)$$

This is an example of the *hyperbolic deformation* of quantum Hamiltonian in the continuous 1D space. If  $\hat{h}(x)$  contains derivatives with respect to  $x$ , the form of  $H$  becomes a complicated one. So, let us introduce explicit construction of the hyperbolic deformation starting from a microscopic Hamiltonian.

Consider a way of introducing the hyperbolic deformation to the lattice systems. We introduce lattice points at  $x = aj$ , where  $a$  is the lattice constant and  $j$  is the lattice index, which runs in a finite range from  $-R/a$  to  $R/a$ . The constant  $R$  we have introduced satisfies  $R/a \gg 1$ , and specifies the size of the system, which ensures a numerical cutoff. Then we have a relation

$$\cosh \nu x = \cosh \nu a j = \cosh \lambda j, \quad (2.4)$$

where  $\lambda = \nu a$  is the deformation parameter that we have used. A discrete analogue of  $H$  in eq. (2.3) is then given by the following lattice Hamiltonian

$$H(\lambda) = \sum_j \cosh \lambda j h_{j,j+1} + \sum_j \cosh \lambda \left(j - \frac{1}{2}\right) g_j, \quad (2.5)$$

where  $h_{j,j+1}$  represents the neighboring interaction,  $g_j$  the on-site ones. Another possible choice of the discrete

Hamiltonian is

$$\begin{aligned} H(\lambda) &= \sum_j \cosh \lambda j h_{j,j+1} \\ &+ \frac{1}{2} \sum_j \left[ \cosh \lambda j + \cosh \lambda(j-1) \right] g_j \\ &= \sum_j \cosh \lambda j h_{j,j+1} + \cosh \frac{\lambda}{2} \sum_j \cosh \lambda(j - \frac{1}{2}) g_j, \end{aligned} \quad (2.6)$$

where the coefficient of the on-site term is different from eq. (2.5). Since we chiefly investigate small  $\lambda$  region, this difference is not conspicuous.<sup>20</sup> We therefore choose  $H(\lambda)$  in the form of eq. (2.5) in the following. It should be noted that the Hamiltonian  $H(\lambda = 0)$  is translationally invariant.

As an example of the 1D lattice systems, let us consider a non-interacting tight-binding model. The deformed Hamiltonian is written as

$$\begin{aligned} H_{\text{TB}}(\lambda) &= -t \sum_j \cosh \lambda j \left( c_j^\dagger c_{j+1} + c_{j+1}^\dagger c_j \right) \\ &- \mu \sum_j \cosh \lambda(j - \frac{1}{2}) c_j^\dagger c_j, \end{aligned} \quad (2.7)$$

where  $t$  represents the hopping amplitude, and  $\mu$  the chemical potential. The operators,  $c_j^\dagger$  and  $c_j$ , appearing in eq. (2.7) are fermion creation and annihilation operators.<sup>21</sup> Since there is no interaction, all the eigenstates can be constructed from one-particle wave functions  $\Psi_j = \langle j | \Psi \rangle$ , where  $|\Psi\rangle$  is a 1-particle eigenstate and  $\langle j |$  is defined as  $\langle 0 | c_j$ . The wave function  $\Psi_j$  of the stationary state satisfies the Schrödinger equation

$$\begin{aligned} E \Psi_j &= -t \cosh \lambda j \Psi_{j+1} - t \cosh \lambda(j-1) \Psi_{j-1} \\ &- \mu \cosh \lambda(j - \frac{1}{2}) \Psi_j. \end{aligned} \quad (2.8)$$

The one-particle ground state energy  $E_0$  becomes zero when  $-\mu/t = 2 \cosh(\lambda/2)$ , and the corresponding wave function  $\Psi_j$  becomes a constant of  $j$ . If  $\mu$  is smaller than  $-2t \cosh(\lambda/2)$ , the ground state wave function is bounded around the origin  $j = 0$ . This kind of bound state is also observed for one particle excitation in many body problem, as we will see in the next section.

Let us check the continuum limit of eq. (2.8). Substituting the relations  $x = aj$ ,  $\lambda = a\nu$  and the correspondence

$$\Psi_j = \Psi(aj) = \Psi(x) \quad (2.9)$$

to eq. (2.8), we obtain the relation

$$\begin{aligned} E \Psi(x) &= \\ &-t \cosh \nu(x - \frac{a}{2}) \cosh \nu \frac{a}{2} [\Psi(x+a) + \Psi(x-a)] \\ &-t \sinh \nu(x - \frac{a}{2}) \sinh \nu \frac{a}{2} [\Psi(x+a) - \Psi(x-a)] \\ &- \mu \cosh \nu(x - \frac{a}{2}) \Psi(x) \end{aligned} \quad (2.10)$$

after some algebra. Expressing the hopping amplitude as  $t = \hbar^2/(2ma^2)$ , chemical potential as  $\mu = -U - 2t$ , and

taking the limit  $a \rightarrow 0$ , we obtain a differential equation

$$E \Psi(x) = \left[ -\frac{\hbar^2}{2m} \frac{\partial}{\partial x} \cosh \nu x \frac{\partial}{\partial x} + U \cosh \nu x \right] \Psi(x). \quad (2.11)$$

The first term in the parenthesis of the r.h.s. is the deformed kinetic energy, and the second term is a kind of trapping potential when  $U > 0$ .

If we consider the imaginary-time dependence of the wave function, the Lagrangian which draws eq. (2.11) from the stationary condition is given by

$$\begin{aligned} \mathcal{L}(\Psi^*, \partial_t \Psi^*, \partial_x \Psi^*, \Psi, \partial_t \Psi, \partial_x \Psi) \\ = \Psi^* \frac{\partial}{\partial \mathbf{t}} \Psi + \cosh \nu x \left[ \frac{\hbar^2}{2m} \frac{\partial \Psi^*}{\partial x} \frac{\partial \Psi}{\partial x} + U \Psi^* \Psi \right] \end{aligned} \quad (2.12)$$

for  $\Psi(x, \mathbf{t})$ , where we have introduced the letter  $\mathbf{t}$  for the imaginary-time variable, and where we have used the unit that satisfies  $\hbar = 1$ . Note that the time-like variable  $\tau$  in eq. (2.1) is related to  $\mathbf{t}$  by the relation  $(\cosh \nu x) d\mathbf{t} = d\tau$ , and in the  $x$ - $\tau$  plane the Lagrangian can be represented as

$$\begin{aligned} \mathcal{L}'(\Psi^*, \partial_\tau \Psi^*, \partial_x \Psi^*, \Psi, \partial_\tau \Psi, \partial_x \Psi) \\ = \cosh \nu x \left[ \Psi^* \frac{\partial}{\partial \tau} \Psi + \frac{\hbar^2}{2m} \frac{\partial \Psi^*}{\partial x} \frac{\partial \Psi}{\partial x} + U \Psi^* \Psi \right], \end{aligned} \quad (2.13)$$

for  $\Psi(x, \tau)$ . The action of the system is given by

$$\begin{aligned} S &= \int \mathcal{L}'(\Psi^*, \partial_\tau \Psi^*, \partial_x \Psi^*, \Psi, \partial_\tau \Psi, \partial_x \Psi) d\tau dx \\ &= \int \left[ \Psi^* \frac{\partial}{\partial \tau} \Psi + \hat{h}(x) \right] (\cosh \nu x) d\tau dx. \end{aligned} \quad (2.14)$$

This action is actually obtained by identifying  $\Psi(x, \tau)$  as a field operator and deriving the path-integral formalism starting from eq. (2.1) with a local Hamiltonian

$$\hat{h}(x) = \frac{\hbar^2}{2m} \frac{\partial \Psi^*}{\partial x} \frac{\partial \Psi}{\partial x} + U \Psi^* \Psi. \quad (2.15)$$

We note that a local deformation of the measure in the action gives the hyperbolic deformation.

### 3. Excitation of the $S = 1$ Heisenberg Chain

We consider the  $S = 1$  antiferromagnetic Heisenberg chain as an example of the 1D many body systems. The system has finite magnetic excitation energy, which is known as the Haldane gap.<sup>3-5</sup> In numerical analyses to obtain the gap of an open-boundary system, there is a custom to put  $S = 1/2$  spins at both ends of the system, in order to avoid the quasi degeneracy in the low-energy states.<sup>13,22</sup> The Hamiltonian of the open-boundary  $S = 1$  chain is represented as

$$\begin{aligned} H(0) &= J \sum_{j=-N+1}^{N-1} \mathbf{S}_j \cdot \mathbf{S}_{j+1} \\ &+ J_{\text{end}} (\mathbf{s}_L \cdot \mathbf{S}_{-N+1} + \mathbf{S}_N \cdot \mathbf{s}_R), \end{aligned} \quad (3.1)$$

which includes  $M = 2N$  numbers of  $S = 1$  spins from  $\mathbf{S}_{-N+1}$  to  $\mathbf{S}_N$ , and the boundary  $S = 1/2$  spins  $\mathbf{s}_L$  and

$\mathbf{s}_R$ . Thus there are  $2N + 2$  spins in total. We count the number of  $S = 1$  spins  $M$  as the size of the system. The parameter  $J > 0$  represents the antiferromagnetic exchange coupling between neighboring  $S = 1$  spins  $\mathbf{S}_j$  and  $\mathbf{S}_{j+1}$ , and  $J_{\text{end}} > 0$  is the coupling at the boundary between  $\mathbf{s}_L$  and  $\mathbf{S}_{-N+1}$  and also between  $\mathbf{S}_N$  and  $\mathbf{s}_R$ . Throughout this article we take  $J$  as the unit of the energy, and use the parameterization  $J_{\text{end}} = J = 1$  unless the value of  $J_{\text{end}}$  is specified.

We introduce the hyperbolic deformation for this system. The deformed Hamiltonian is represented as

$$H(\lambda) = J \sum_{j=-N+1}^{N-1} \cosh \lambda j \mathbf{S}_j \cdot \mathbf{S}_{j+1} \quad (3.2)$$

$$+ J_{\text{end}} \cosh \lambda N (\mathbf{s}_L \cdot \mathbf{S}_{-N+1} + \mathbf{S}_N \cdot \mathbf{s}_R) .$$

When  $\lambda = 0$ , eq. (3.2) becomes eq. (3.1). Occasionally it is convenient to treat a system that contains odd number of spins, so that one of the  $S = 1$  spin is just at the center of the system. In order to satisfy the condition, we introduce another type of the deformed system described by the Hamiltonian

$$H(\lambda) = J \sum_{j=-N+1}^{N-2} \cosh \lambda (j - \frac{1}{2}) \mathbf{S}_j \cdot \mathbf{S}_{j+1} \quad (3.3)$$

$$+ J_{\text{end}} \cosh \lambda (N - \frac{1}{2}) (\mathbf{s}_L \cdot \mathbf{S}_{-N+1} + \mathbf{S}_{N-1} \cdot \mathbf{s}_R) ,$$

where there are  $2N + 1$  spins in total. In this case the system size, which is the number of  $S = 1$  spins, is  $M = 2N - 1$ .

### 3.1 Gap estimation for the undeformed system

We first estimate the value of the Haldane gap  $\Delta$  for undeformed systems  $\lambda = 0$ , in order to get reference data for the later study under deformation  $\lambda > 0$ . The excitation energy from the ground state is calculated by the DMRG method,<sup>9-12</sup> as a function of  $J_{\text{end}}$ , the system size  $M = 2N$  (or  $2N - 1$ ), and the number of states kept  $m$ , which is increased up to 180. From the various values of  $J_{\text{end}}$  for which we have performed calculations, we show the data for two typical values  $J_{\text{end}} = 0.5088$  and  $J_{\text{end}} = 0.50866$  in Table I. The former value is used in a literature<sup>13</sup> and the latter is an optimized one in this work.

The data for  $J_{\text{end}} = 0.5088$  in Table I are calculated under the same conditions as them<sup>13</sup> except for a readjustment of the energy origin. For precise determination of the lowest eigenvalue, we shift the origin of the energy so that the ground-state energy becomes nearly zero. This energy shift is realized by the following process. First we obtain the ground state  $|\Psi_0\rangle$  diagonalizing the Hamiltonian in eq. (3.2) or eq. (3.3), and calculate the nearest neighbor correlation function  $w_{i,i+1} = \langle \Psi_0 | \mathbf{S}_i \cdot \mathbf{S}_{i+1} | \Psi_0 \rangle$ . We then replace the neighboring interaction  $\mathbf{S}_i \cdot \mathbf{S}_{i+1}$  in the Hamiltonian by  $\mathbf{S}_i \cdot \mathbf{S}_{i+1} - w_{i,i+1} \hat{I}$  with an identity operator  $\hat{I}$ , and perform the same subtraction also for the boundary terms where  $\mathbf{s}_L$  and  $\mathbf{s}_R$  are involved. This subtraction can be performed successively when one constructs the renormalized Hamiltonians  $H_L$

Table I. Calculated excitation energy  $\Delta_M$  for each system with the size  $M$ , which is the number of  $S = 1$  spins. The integer  $m$  is the number of states kept. The interaction strength at the system boundary is  $J_{\text{end}} = 0.5088$  (the upper series from  $M = 2N = 100$  to 160) or  $J_{\text{end}} = 0.50866$  (the lower series). Truncation errors  $1 - P_{\text{GS}}(m)$  and  $1 - P_{\text{EX}}(m)$  are also shown for the ground and the 1st excited states, respectively. (See text.)

$M$	$m$	$\Delta_M$	$1 - P_{\text{GS}}(m)$	$1 - P_{\text{EX}}(m)$
100	120	0.4104951946	5.196E-12	7.724E-10
	140	0.4104949559	1.445E-12	3.009E-10
	160	0.4104948683	3.579E-13	1.556E-10
	180	0.4104948265	4.170E-14	6.870E-11
120	120	0.4104929134	5.194E-12	8.192E-10
	140	0.4104926043	1.446E-12	3.237E-10
	160	0.4104924896	3.769E-13	1.657E-10
	180	0.4104924345	4.125E-14	7.301E-11
140	120	0.4104912749	5.197E-12	8.539E-10
	140	0.4104908951	1.445E-12	3.300E-10
	160	0.4104907533	3.678E-13	1.732E-10
	180	0.4104906847	4.270E-14	7.615E-11
160	120	0.4104900535	5.193E-12	8.770E-10
	140	0.4104896021	1.443E-12	3.391E-10
	160	0.4104894323	3.695E-13	1.799E-10
	180	0.4104893502	5.500E-14	7.854E-11
100	160	0.4104803729	3.657E-13	1.562E-10
	180	0.4104803310	3.373E-13	6.875E-11
120	160	0.4104802346	3.692E-13	1.663E-10
	180	0.4104801793	4.313E-14	7.306E-11
140	160	0.4104801400	3.904E-13	1.738E-10
	180	0.4104800712	4.351E-14	7.620E-11
160	160	0.4104800736	3.690E-13	1.798E-10
	180	0.4104799915	6.541E-14	7.858E-11

and  $H_R$  for the left and the right block of the system during the finite-size sweeping process. The ground-state energy of the shifted Hamiltonian thus obtained is nearly zero. The total amount of the energy shift can be obtained from  $w_{i,i+1}$ . It should be noted that the above energy shift process is important for the large-scale system, where the ground-state energy becomes a big number. In the same manner, we have to use the shifted Hamiltonian when we consider the hyperbolically deformed system with  $\lambda > 0$ , where the absolute value of the ground-state energy increases exponentially with the system size.

Truncation errors introduced to the ground state  $1 - P_{\text{GS}}(m)$ , which are listed in Table I, are calculated by the following standard procedures in DMRG calculation. After sufficient numbers of finite size sweeping, we obtain the optimized variational ground state

$$|\tilde{\Psi}\rangle = \sum_{\xi_l, S_l^z, S_l^z \xi_r} \tilde{\Psi}_{\xi_l, S_l^z, S_l^z \xi_r} |\xi_l\rangle |S_l^z\rangle |S_l^z \xi_r\rangle, \quad (3.4)$$

where  $|\xi_l\rangle$  and  $|\xi_r\rangle$  represent relevant block spin state for the left and the right blocks, respectively, that take at most  $m$  numbers of states. Creating the reduced density matrix for the left half of the system

$$\rho_{\xi_l, S_l^z; \xi_l' S_l^z} = \sum_{S_l^z \xi_r} \tilde{\Psi}_{\xi_l, S_l^z, S_l^z \xi_r}^* \tilde{\Psi}_{\xi_l' S_l^z, S_l^z \xi_r}, \quad (3.5)$$

and diagonalizing it to obtain eigen values  $w_\alpha$ , where we assume the ascending order for  $w_\alpha$ . The truncation error

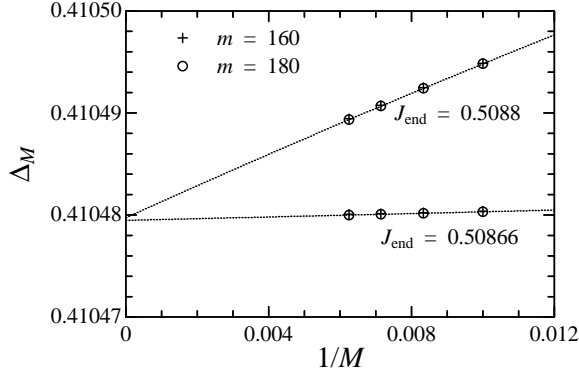


Fig. 2. System size dependence of the excitation gap  $\Delta_M$  listed in Table I. Only data for  $m = 160$  and  $m = 180$  is given.

is then calculated as

$$1 - P_{\text{GS}}(m) = 1 - \sum_{\alpha=1}^m w_{\alpha}. \quad (3.6)$$

The truncation error for the lowest excited state  $1 - P_{\text{EX}}(m)$  is also calculated in the same manner, using the optimized ground-state in the subspace where the total number of  $S^Z$  is equal to 1.

Figure 2 shows the system size dependence of the excitation gap, which is given as a list in Table I. For both cases,  $J_{\text{end}} = 0.5088$  and  $J_{\text{end}} = 0.50866$ , the gap is nearly linear in  $1/M = 1/(2N)$ . From the numerical data under the condition  $m = 160$ , we obtain  $\Delta = 0.41047970(1)$  when  $J_{\text{end}} = 0.5088$  and  $\Delta = 0.41047968(2)$  when  $J_{\text{end}} = 0.50866$  by use of the fitting with respect to second order polynomials, where the numbers shown in the parenthesis are the mean-square fitting error. These two values of the gap seem to be consistent, however, the gap is sensitive to the value of  $m$ . From the data when we keep  $m = 180$  states, we obtain  $\Delta = 0.41047947(1)$  when  $J_{\text{end}} = 0.5088$  and  $\Delta = 0.41047944(1)$  when  $J_{\text{end}} = 0.50866$ . So far as we have calculated, the estimated value of  $\Delta$  is always a decreasing function of  $m$ . This tendency is also discussed in the last section. Indeed, when  $J_{\text{end}} = 0.5088$ , the values are  $\Delta = 0.41048145(9)$  for  $m = 120$ ,  $\Delta = 0.41048019(4)$  for  $m = 140$ ,  $\Delta = 0.41047970(1)$  for  $m = 160$ , and  $\Delta = 0.41047947(1)$  for  $m = 180$ . In this parameter range of  $m$ , change in  $\Delta$  as a function of  $m$  is bigger than the error in the last digit of the above estimation. Thus the lowest value obtained so far can be regarded as the upper bound for  $\Delta$ . We therefore use the smallest value  $\Delta = 0.41047944$  when  $m = 180$  and  $J_{\text{end}} = 0.50866$  as the better estimation of the upper bound of  $\Delta$  than the estimation of  $m = 180$  and  $J_{\text{end}} = 0.5088$ .

Note that the condition  $J_{\text{end}} = 0.50866$  is valid only for the Hamiltonians shown in Eqs. (3.2) and (3.3). If we need the excitation gap for a variety of  $S = 1$  spin chains, which contain anisotropy and biquadratic terms, we have to find another appropriate value of  $J_{\text{end}}$  for each cases.

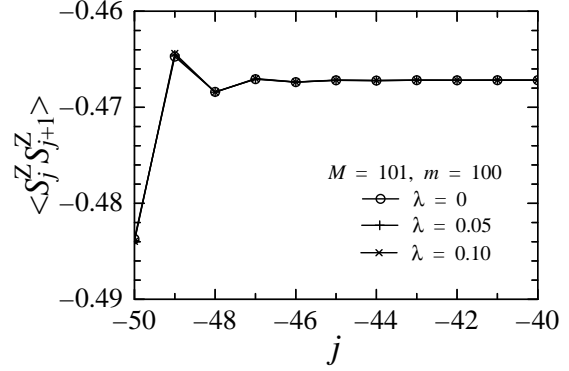


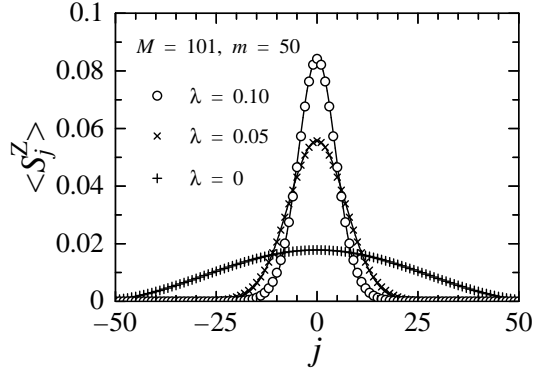
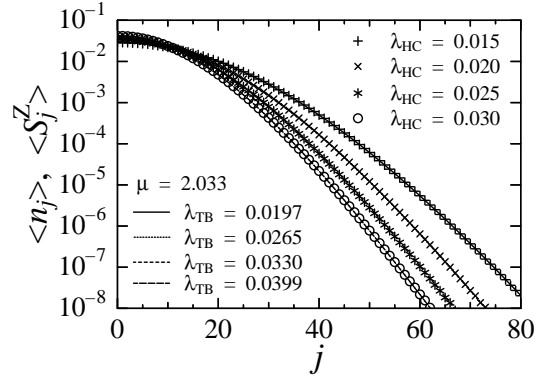
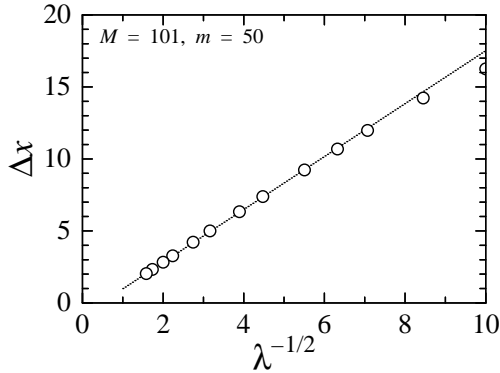
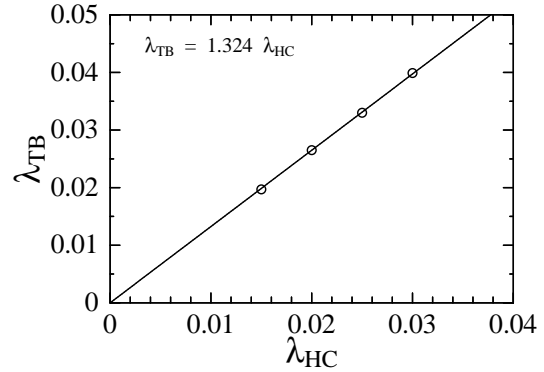
Fig. 3. Nearest neighbor spin correlation function  $\langle S_j^Z S_{j+1}^Z \rangle$  of the singlet ground state when the system size is  $M = 2N - 1 = 101$ .

### 3.2 Bounded excitation when $\lambda > 0$

Let us observe the ground state and the elementary excitation of the deformed chain, which is described by the Hamiltonian in eq. (3.2) or eq. (3.3) with  $\lambda > 0$ . Figure 3 shows the nearest-neighbor spin correlation functions between  $S = 1$  spins  $\langle S_j^Z S_{j+1}^Z \rangle$  of the singlet ground state when the system size is  $M = 2N - 1 = 101$ . In Fig. 3, we look only at the boundary of the system, where local fluctuation of this correlation function is prominent. It is known that the hyperbolic deformation has an effect of decreasing the correlation length  $\xi$ .<sup>15</sup> In the  $S = 1$  antiferromagnetic Heisenberg spin chain,  $\xi$  is of the order of unity already at  $\lambda = 0$ , and thus the effect of hyperbolic deformation is not conspicuous in long-range correlation functions, as long as the ground state is concerned. As displayed in Fig. 3, the short-range correlation function is also not affected by the deformation in this parameter range of  $\lambda$ . Although the interaction strength is position dependent, the spin correlation function is almost uniform inside the system. Thus we may say that the vacuum of the quasiparticle excitation is kept fixed in its internal structure against the deformation. This behavior is favorable to have a good convergence in the energy gap of the elementary excitation.

Next, we observe the magnetic excitation. Figure 4 shows the Z-component of the local spin polarization  $\langle S_j^Z \rangle$  calculated for the first excited state, which is the lowest-energy state in the subspace where the total  $S^Z$  of the system is unity. The polarization  $\langle S_j^Z \rangle$  is positive everywhere, unless one chooses an extremely large  $\lambda$ . Thus it is possible to regard  $\langle S_j^Z \rangle$  as the distribution probability of the excited magnetic quasiparticle. The quasiparticle is bounded around the center of the system when  $\lambda = 0.05$  and  $0.10$ , in contrast to the unbounded case when  $\lambda = 0$ .

The observed quasiparticle distribution in Fig. 4 is close to the Gaussian distribution around the origin  $j = 0$ , when  $\lambda = 0.05$  or  $0.10$ . In order to quantify the

Fig. 4. Spin polarization  $\langle S_j^Z \rangle$  of the first excited state.Fig. 6. Comparison between  $\langle n_j \rangle$  of the tight-binding model and  $\langle S_j^Z \rangle$  of the Heisenberg chain.Fig. 5. The distribution width  $\Delta x$  of the quasiparticle with respect to  $1/\sqrt{\lambda}$ .Fig. 7. Linear dependence between  $\lambda_{\text{TB}}$  and  $\lambda_{\text{HC}}$ .

distribution width, we introduce

$$\Delta x = \sum_{j=-N+1}^{N-1} \sqrt{j^2 \langle S_j^Z \rangle} \quad (3.7)$$

for the cases when the system size is odd. Figure 5 shows the value of  $\Delta x$  calculated for the 101-site system. The dotted line is the fitting for those  $\Delta x$  in the range  $\lambda^{-1/2} \leq 4$ , equivalently  $\lambda \geq 0.04$ . The distribution width  $\Delta x$  is proportional to  $1/\sqrt{\lambda}$  in this parameter region of  $\lambda$ , where  $\Delta x$  is almost independent of the system size. We have confirmed that the relation  $\Delta x \propto 1/\sqrt{\lambda}$  holds for  $1/\sqrt{\lambda} \leq 20$ , equivalently  $\lambda \geq 0.0025$ , when the system size is  $M = 2N = 1000$ . If  $\lambda$  becomes too small for a fixed system size,  $\Delta x$  deviates from the fitting line due to the finite size effect. The deviation of  $\Delta x$  from the  $1/\sqrt{\lambda}$  behavior suggests breaking the confinement of the quasiparticle.

To speak qualitatively, the observed  $\lambda$ -dependence of  $\Delta x$  is consistent with the effective one-particle potential

$$U(j) = J \cosh \lambda j \sim J + \frac{J}{2} (\lambda j)^2 \quad (3.8)$$

in the neighborhood of the origin  $j = 0$ . Note that a large system size  $M$  ensures existence of a finite central region of the chain satisfying  $\lambda j \ll 1$  for small but finite

$\lambda$ . Thus in a final simulation, we need to have an enough size  $M \sim 1000$ , which is tractable by the DMRG method at present.

It is possible to interpret the relation  $\Delta x \sqrt{\lambda} \sim \text{const.}$  as the quantum mechanical uncertainty for the excited quasiparticle under this harmonic potential. The quasiparticle distribution in Fig. 4 can be explained quantitatively by means of the tight-binding model given in eq. (2.7). Let us consider the occupation number  $\langle n_i \rangle = \langle c_j^\dagger c_j \rangle$  for the lowest energy one-particle state. It is possible to obtain a good approximation of  $\langle S_j^Z \rangle$  by  $\langle n_i \rangle$  if we choose the parametrization  $t = 1$  and  $\mu = 2.033$ . Figure 6 shows the correspondence between  $\langle S_j^Z \rangle$  and  $\langle n_i \rangle$ , where  $\lambda_{\text{HC}}$  represents the deformation parameter for the spin chain and  $\lambda_{\text{TB}}$  that for the tight-binding model. The value of  $\lambda_{\text{TB}}$  is determined so as to have a best fit of  $\langle S_j^Z \rangle$  and  $\langle n_i \rangle$ . Figure 7 shows the relation between  $\lambda_{\text{TB}}$  and  $\lambda_{\text{HC}}$ . We can see that a simple relation  $\lambda_{\text{TB}} = 1.324 \lambda_{\text{HC}}$  holds, where the proportional constant 1.324 gives the correction to the qualitative description in eq. (3.8).

#### 4. Gap Estimation by Extrapolation in $\lambda$

We have observed that the magnetic excitation of the hyperbolically deformed  $S = 1$  Heisenberg chain is

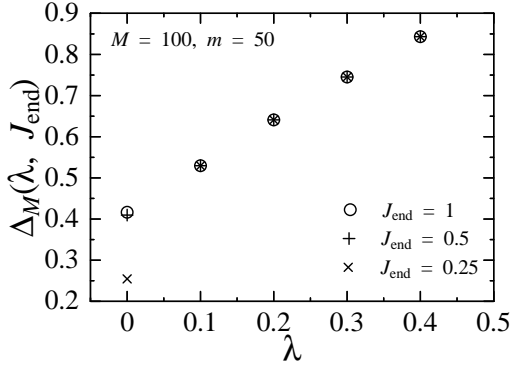


Fig. 8. Excitation energy  $\Delta_M(\lambda, J_{\text{end}})$  for the 100-site system when  $J_{\text{end}} = 0.25, 0.5,$  and  $1$ .

bounded around the center of the system. In this section we focus on the excitation energy

$$\Delta(\lambda) = E_1(\lambda) - E_0(\lambda) \quad (4.1)$$

and investigate its dependence on  $\lambda$ . Here,  $E_0(\lambda)$  is the ground-state energy and  $E_1(\lambda)$  is the energy of the first excited state. As it is shown in the following,  $\Delta(\lambda)$  is insensitive to the boundary interaction parameter  $J_{\text{end}}$ .

#### 4.1 Insensitivity of $\Delta(\lambda)$ with respect to $J_{\text{end}}$

Figure 8 shows  $\Delta_M(\lambda, J_{\text{end}})$  for the 100-site system, where  $\Delta_M(\lambda, J_{\text{end}})$  is the calculated gap for the  $M$ -site system when the boundary interaction is  $J_{\text{end}}$ . We have chosen the set of deformation parameter  $\lambda = 0, 0.1, 0.2, 0.3,$  and  $0.4$ , with  $J_{\text{end}} = 0.25, 0.5,$  and  $1$ . When  $\lambda = 0$ , the gap  $\Delta_{100}(0, J_{\text{end}})$  is dependent on the value of  $J_{\text{end}}$ . This is because the excited quasiparticle can reach the system boundary, and it is affected by the effect of  $J_{\text{end}}$ . In particular, when  $\lambda = 0$  and  $J_{\text{end}} = 0.25$  the quasiparticle is even localized near the system boundary. Appearance of this surface excitation tells that we need to avoid a parameter range of  $\lambda \ll 0.1$  with  $J_{\text{end}} = 0.25$ .

On the other hand when  $\lambda \geq 0.1$ , the excited quasiparticle cannot reach the system boundary as shown in Fig. 4, and the effect of  $J_{\text{end}}$  on  $\Delta_{100}(\lambda, J_{\text{end}})$  is negligible for this excitation. In this way, the hyperbolic deformation has an effect of separating elementary excitations from the system boundary.

To fix a desirable parameter range of  $M$  and  $\lambda$ , in order to decouple quasiparticle from the boundary, let us observe the system size dependence of  $\Delta_M(\lambda, J_{\text{end}})$  for the case  $\lambda = 0.0025$ , which is the smallest one used in the following analysis. The system size is increased up to  $M = 2N = 1000$ . We introduce a quantity judging an error

$$\epsilon_\Delta = \left| \frac{\Delta_M(\lambda, J_{\text{end}})}{\Delta_{1000}(\lambda, 0.25)} - 1 \right| \quad (4.2)$$

In the parameter region where  $\epsilon_\Delta$  is close to zero, we can say that the boundary effect is removed. Figure 9 shows  $\Delta_M(0.0025, J_{\text{end}})$  with respect to  $1/M = 1/2N$  at  $J = 0.25, 0.5$  and  $1$ . When  $J_{\text{end}} = 0.25$  and

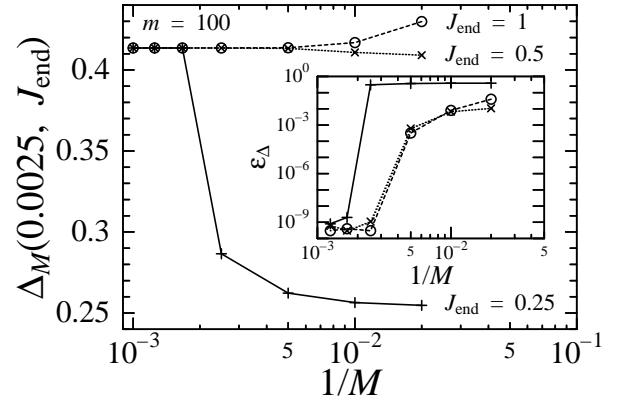


Fig. 9. Excitation energy  $\Delta_M(0.0025, J_{\text{end}})$  as a function of  $1/M = 1/(2N)$  under the condition  $J_{\text{end}} = 0.25, 0.5,$  and  $1$ . The inset shows  $\epsilon_\Delta$  in eq. (4.2).

when the system size is small, the boundary excitation is detected as appearance of smaller gap around  $\Delta_M(0.0025, 0.25) \simeq 0.26$ . Because the strength of the boundary interaction is  $J_{\text{end}} \cosh \lambda N$ , the energy of the boundary excitation increases with the system size. Finally the bulk excitation  $\Delta(\lambda = 0.0025)$  is detected as a gap of  $\Delta_M(0.0025, J_{\text{end}}) \simeq 0.41$  in the neighborhood of  $M = 2N = 1000$ . From  $\epsilon_\Delta$  shown in the inset, we can say that the effect of  $J_{\text{end}}$  to  $\Delta_M(\lambda, J_{\text{end}})$  is less than  $10^{-9}$  when the system size reaches 1000. Note that  $\epsilon_\Delta$  is greater than  $10^{-10}$  since we set the convergence threshold of the eigensolver, which is used in the finite-size sweeping process, to the value  $10^{-8}$ . When it is necessary, we decrease the threshold down to  $10^{-10}$  in the following numerical calculations.

#### 4.2 $\lambda$ dependence of the energy gap

We have erased the effect of system boundary from the elementary excitation by the hyperbolic deformation. Thus the estimation process for the Haldane gap  $\Delta$  is reduced to the extrapolation of  $\Delta(\lambda)$  with respect to the deformation parameter  $\lambda$ . As we will see, the difference  $\Delta(\lambda) - \Delta(0)$  is nearly proportional to  $\lambda$ , where the dependence is consistent with the picture of the shallow bound state appearing in §3.

In the following analysis, we use  $\Delta_{600}(\lambda, 1)$  as the bulk excitation  $\Delta(\lambda)$ , because the estimation value  $\Delta_M(\lambda, 1)$  is not changed within numerical precision we require when the system size  $M$  runs from 600 to 1000. Fitting 2nd-order polynomials to the shown data, we obtain  $\Delta(0) = 0.41047941(1)$  when  $m = 160$  and  $\Delta(0) = 0.41047931(1)$  when  $m = 180$ , where the numbers in the parenthesis represent the fitting error. As we have discussed, we may choose the smaller one  $\Delta(0) = 0.41047931$  as the estimated upper bound of the Haldane gap  $\Delta$ .

Let us check the precision of the value  $\Delta(0) = 0.41047931(1)$  that we have obtained from the independent data analysis. Let us assume that  $\Delta(\lambda)$  can be rep-

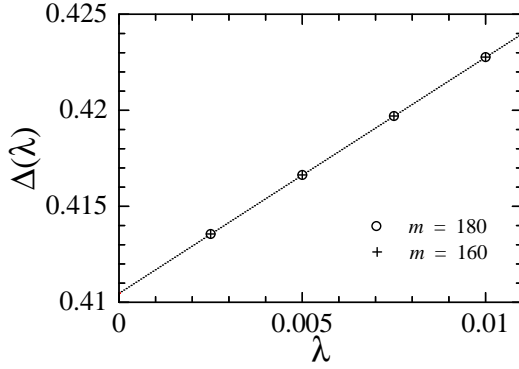


Fig. 10. Excitation energy  $\Delta(\lambda)$  when  $J_{\text{end}} = 1$ . The dotted line shows the result of fitting to the second-order polynomial.

resented in terms of a polynomial in  $\lambda$

$$\Delta(\lambda) = \Delta(0) + a\lambda + b\lambda^2 + O(\lambda^3). \quad (4.3)$$

A way of estimating  $\Delta(0)$  efficiently is to consider the derivative between two values of deformation parameters

$$\frac{\lambda_2 \Delta(\lambda_1) - \lambda_1 \Delta(\lambda_2)}{\lambda_2 - \lambda_1} = \Delta(0) - b\lambda_1\lambda_2 + O(\lambda^3), \quad (4.4)$$

which does not contain first order term in  $\lambda$ . Introducing the notation  $\lambda' = (\lambda_2 + \lambda_1)/2$  and  $\delta = (\lambda_2 - \lambda_1)/2$ , this derivative can be written as

$$\Delta(0) - b(\lambda'^2 - \delta^2) + O(\lambda'^3) = \tilde{\Delta}(\lambda', \delta). \quad (4.5)$$

Using the data shown in Fig. 10, we calculate  $\tilde{\Delta}(\lambda', \delta)$  for neighboring  $\lambda$ s and plot the result in Fig. 11. It is obvious that the third order correction  $O(\lambda'^3)$  is very small in the shown parameter area, and  $\tilde{\Delta}(\lambda', \delta)$  is almost linear in  $\lambda'^2 - \delta^2$ . By use of linear extrapolation we obtain  $\Delta(0) = 0.41047940(2)$  when  $m = 160$  and  $\Delta(0) = 0.41047931(1)$  when  $m = 180$ , where we have shown the fitting error in the parenthesis. As we have done for the previous estimation for the upper bound, considering  $m$ -dependence of the value, we choose  $\Delta(0) = 0.41047931$  as the candidate. This value is the same as the number obtained in the previous paragraph.

## 5. Gap Estimation by the Sequence Interval Squeeze Method

In this section, we present another new result on upper and lower bounds of the true Haldane gap using an examination of numerical-diagonalization data. The reason for the usage of the numerical-diagonalization technique is to keep the high precision in the original numerical data. Having an independent estimate by a complementary approach to the DMRG calculation, we obtain definite values on two bounds, which are concluded in the last section.

Quite recently Nakano, one of the authors, and Terai proposed a new way to create an increasing (decreasing) sequence from monotonically decreasing (increasing) sequences of numerical data, which was immediately applied to estimation of the Haldane gap with high accuracy.<sup>8</sup> A noticeable superiority of their analysis is

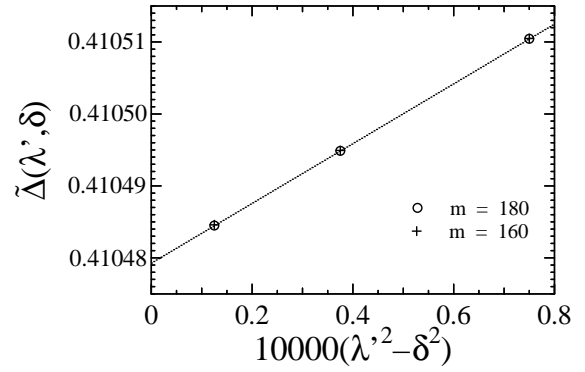


Fig. 11.  $\tilde{\Delta}(\lambda', \delta)$  in eq. (4.5) with respect to  $\lambda'$ . The dotted line represents the linear fitting.

that the method enables one to estimate a lower (upper) bound simultaneously with an upper (lower) bound of the gap.

Here, we review this estimation method. First, we consider the initial sequence  $A_M^{(0)}$  for  $M = 2, 4, 6, \dots$ , which is convergent to  $A_\infty^{(0)}$ . Suppose that we can generate  $A_M^{(k)}$  for  $k = 1, 2, 3, \dots$  from  $A_M^{(0)}$  by some method so that the new sequences  $A_M^{(k)}$  have the same limit, namely  $A_\infty^{(k)} = A_\infty^{(0)}$  for all  $k$ . Supposed also that the set of the sequences  $A_M^{(k)}$  has the following properties,

- (i)  $A_M^{(k)}$  is monotonic with respect to  $M$ .
- (ii)  $\xi_M^{(k)}$  increases with  $M$ ;  $\xi_{M+2}^{(k)} > \xi_M^{(k)}$ ,
- (iii)  $\xi_M^{(k)}$  decreases with  $k$ ;  $\xi_M^{(k+1)} < \xi_M^{(k)}$ ,

where  $\xi$  is the decay length<sup>7</sup> given by

$$\xi_M^{(k)} = 2 / \log \left( \frac{A_{M-4}^{(k)} - A_{M-2}^{(k)}}{A_{M-2}^{(k)} - A_M^{(k)}} \right). \quad (5.1)$$

Nakano and Terai introduced another sequence<sup>8</sup> obtained from the sequences  $A_M^{(k')}$  and  $A_M^{(k)}$  which are convergent to  $A_\infty^{(0)}$  from the same side. The new sequence  $B_M^{(k)}$  is given by

$$B_{M+1}^{(k)} = \frac{A_M^{(k)} A_{M+2}^{(k')} - A_{M+2}^{(k)} A_M^{(k')}}{A_{M+2}^{(k')} - A_M^{(k')} - A_{M+2}^{(k)} + A_M^{(k)}}, \quad (5.2)$$

for  $k > k'$ . The most important property of  $B_M^{(k)}$  is that the new sequence is convergent to the same limit  $A_\infty^{(0)}$  from the *opposite* side. (See appendix in ref. [8].) Thus, there is a relation  $B_{M_1}^{(k_1)} < A_\infty^{(0)} < A_{M_2}^{(k_2)}$  (or  $A_{M_1}^{(k_1)} < A_\infty^{(0)} < B_{M_2}^{(k_2)}$ ) and we obtain a reliable interval including the limit  $A_\infty^{(0)}$ , which we would like to know. Here  $k_1, k_2, M_1$  and  $M_2$  are integers. When the sequences  $A_M^{(k)}$  and  $A_M^{(k')}$  are monotonically decreasing,  $\min_{k,M}(A_M^{(k)})$  and  $\max_{k,M}(B_M^{(k)})$  are an upper bound and a lower one for  $A_\infty^{(0)}$ , respectively. When the direction of  $A_M^{(k)}$  and  $A_M^{(k')}$  is opposite,  $\max_{k,M}(A_M^{(k)})$  and



$\min_{k,M}(B_M^{(k)})$  give a lower bound and an upper one, respectively.

An appropriate set of the sequences  $A_M^{(k)}$  can be generated systematically from  $A_M^{(0)}$  to make the interval narrower by using convergence-acceleration techniques. As such a technique, we discuss the  $\varepsilon$ -algorithm<sup>7,23</sup> and its generalization. The  $\varepsilon$ -algorithm provides us with a new sequence of one-level higher, by the relation between the neighboring three levels

$$\frac{1}{A_M^{(k+1)} - A_{M-2}^{(k)}} \quad (5.3)$$

$$= \frac{1}{A_{M-4}^{(k)} - A_{M-2}^{(k)}} + \frac{1}{A_M^{(k)} - A_{M-2}^{(k)}} - \frac{\alpha}{A_{M-4}^{(k-1)} - A_{M-2}^{(k)}},$$

for  $\alpha = 1$ . This algorithm for  $\alpha = 1$  was originally developed by Wynn.<sup>23</sup> In order to create the first level sequence  $A_M^{(1)}$ , we can prepare a dummy sequence  $A_M^{(-1)}$  of the level  $-1$ , where all of the elements are infinitely large, namely  $A_M^{(-1)} = \infty$ .

To know whether the acceleration is successful or not, the monitoring of the decay length given by eq. (5.1) is important. One can consider that the convergence of a transformed sequence  $A_M^{(k)}$  for  $k \geq 1$  is successfully accelerated when all the above conditions (i)-(iii) hold.

We put the excitation gap of the  $M$ -site  $S = 1$  chain  $\mathcal{H} = \sum_{i=1}^M \mathbf{S}_i \cdot \mathbf{S}_{i+1}$  under a certain boundary condition into the initial sequence  $A_M^{(0)}$ . Note that the direction of the monotonic behavior of the sequence depends on the boundary condition adopted. If we impose the periodic ( $\mathbf{S}_{M+1} = \mathbf{S}_1$ ) or the twisted ( $S_{M+1}^x = -S_1^x, S_{M+1}^y = -S_1^y, S_{M+1}^z = S_1^z$ ) boundary condition, the direction is different with each other.<sup>8</sup> What we would like to do is to estimate  $A_\infty^{(0)}$  only from a finite part of the initial sequence.

For long, only the systems under the periodic boundary condition were examined in most of the finite-size-scaling studies based on numerical diagonalization data. Finite-size gap of such systems usually decreases monotonically, when the system size is increased. If we apply the  $\varepsilon$ -algorithm to the monotonically decreasing sequence, we obtain only upper bounds of the Haldane gap. Nakano and Terai found that the excitation gap of the finite size systems under the twisted boundary condition is monotonically increasing.<sup>8</sup> Thus, we should examine which is better among both of the boundary conditions, periodic and twisted.

We can interpret that Nakano and Terai found a quite systematic approach to overcome limitation of the usage of the original  $\varepsilon$ -algorithm.<sup>8</sup> Fundamental steps are summarized as usage of 1) examination of different boundary conditions, 2) acceleration of the monotonic sequences  $A_M^{(k)}$ , and 3) the above new sequence  $B_M^{(k)}$ . If an appropriate acceleration transformation is chosen, one easily obtains a reliable interval including the limit  $A_\infty^{(0)}$ , which we would like to know. The interval gets narrower as the number of initial data is increased. Hereafter, we call the above procedure the sequence interval squeeze (SIS) method. Getting the bounds of both sides, we can quantitatively discuss the precision of the estimates of the

Table II. Sequence of finite-size gaps by eq. (5.3) with  $\alpha = 0.4$ .

$M$	$A_M^{(2)}$	$\xi_M^{(2)}$	$A_M^{(3)}$	$\xi_M^{(3)}$
12	0.409599020			
14	0.410158700			
16	0.410354714	1.91	0.410442366	
18	0.410427448	2.02	0.410465180	
20	0.410456146	2.15	0.410473181	1.91
22	0.410468261	2.32	0.410476497	2.27
24	0.410473733	2.52	0.410477982	2.49
$M$	$A_M^{(4)}$	$\xi_M^{(4)}$	$A_M^{(5)}$	
20	0.410476976			
22	0.410478577			
24	0.410479051	1.64	0.410479218	

Table III. Antimonotonic sequence  $B_M^{(k)}$  for  $\alpha = 0.4$ .

$M$	$B_M^{(2)}$	$B_M^{(3)}$	$B_M^{(4)}$
13	0.411197171		
15	0.410724641		
17	0.410568330	0.410491523	
19	0.410513257	0.410482576	
21	0.410492985	0.410480499	0.410480148
23	0.410485151	0.410479829	0.410479554

Haldane gap that were reported so far.

Nakano and Terai substituted the excitation gap of the finite size systems under the twisted boundary condition for  $A_M^{(0)}$ ; the initial sequence is monotonically increasing. From the numerical data collected up to  $A_{M=24}^{(0)}$  with the twisted boundary condition, the SIS method provides us with the estimate  $\Delta = 0.4104789(13)$  as the Haldane gap from the acceleration process under  $\alpha = 1$ .

Let us recall that an available acceleration transformation is not limited to the  $\varepsilon$ -algorithm with  $\alpha = 1$ . Actually, the first step of  $\varepsilon$ -algorithm is equivalent to the Aitken-Shanks transformation,<sup>24</sup> which corresponds to  $\alpha = 0$ . If one takes  $\alpha = 0$  for the second step and the later, the transformation (5.3) is reduced to just an iteration of the Aitken-Shanks transformation. Other choices of  $\alpha$  for the second step and the later correspond to different convergence acceleration transformations, on each of which the degree of acceleration depends. Thus we may optimize the convergence acceleration in the step 2) in the SIS method. If we adjust  $\alpha$  within a range in which the above three conditions are certified, the strength of the acceleration can be optimized. In the present work, we apply  $\alpha = 0.4$  in eq. (5.3) giving  $A_M^{(k)}$  and  $k' = k - 2$  in eq. (5.2) giving  $B_M^{(k)}$  to the same numerical data with the twisted boundary condition. The result successfully gives an inside interval narrower than the result obtained by  $\alpha = 1$ .

Let us list all the  $A_M^{(k)}$  created by eq. (5.3) in Table II. Sequences  $A_M^{(0)}$  and  $A_M^{(1)}$  are not presented because they do not change due to a variance of  $\alpha$ . As it is observed,  $A_M^{(k)}$  and  $\xi_M^{(k)}$  satisfy the set of the three conditions for the successful convergence acceleration. We then create another sequence  $B_M^{(k)}$  by eq. (5.2) and show them in Table III. One can clearly observe that

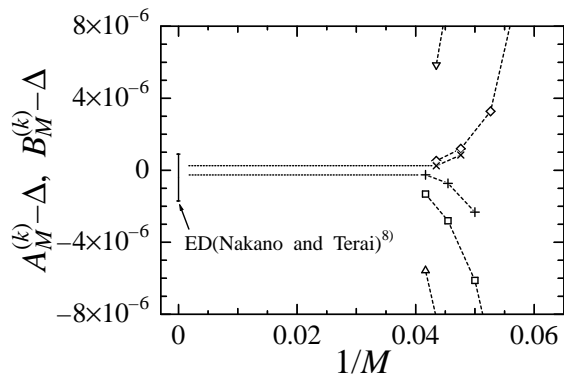


Fig. 12. Convergence of the data shown in Table II and III with respect to  $M$ . We use the common shift  $\Delta = 0.4104793$  for display. Triangles, squares, and pluses denote  $A_M^{(2)}$ ,  $A_M^{(3)}$ , and  $A_M^{(4)}$ , respectively. Reversed triangles, diamonds, and crosses denote  $B_M^{(2)}$ ,  $B_M^{(3)}$ , and  $B_M^{(4)}$ , respectively.

$B_M^{(k)}$  is monotonically convergent from the side opposite to  $A_M^{(k)}$ . Figure 12 depicts the  $1/M$  dependence of these sequences. The present result gives a new interval  $[0.410479051, 0.410479554]$  for an estimate for the Haldane gap  $\Delta$ , which is narrower than the reported one in ref. [8].

## 6. Conclusions and Discussions

We have observed the magnetic excitation of the  $S = 1$  Heisenberg chain, whose exchange coupling is deformed hyperbolically. The magnetic quasiparticle is weakly bounded in the neighborhood of the center of the system. It is shown that the excitation energy  $\Delta(\lambda)$  is nearly linear in  $\lambda$ , and the extrapolation to  $\lambda = 0$  gives an estimate of the Haldane gap, as precise as that obtained by the SIS method. Since the quasiparticle does not reach the system boundary under the hyperbolic deformation, one does not have to pay special attention to the boundary interaction strength.

Here, let us summarize the estimated values of the Haldane gap we have obtained with those reported so far. Figure 13 shows  $\Delta(0)$  obtained by

- A. Lanczos method + convergence acceleration in ref. [25]
- B. DMRG applied to undeformed system in ref. [13]
- C. Monte Carlo simulation in ref. [26]
- D. Lanczos method + SIS in ref. [8]
- E. DMRG applied to undeformed system in §3.
- F. Deformation analysis in §4 with polynomial fitting.
- G. Deformation analysis in §4 with derivatives.
- H. Lanczos method + SIS in §5.

Each method among E at  $J_{\text{end}} = 0.5088$ , F, G has four data points when  $m = 120, 140, 160$  and  $180$ . In addition, there are two data points under the conditions  $m = 160$  and  $180$  for the method E at  $J_{\text{end}} = 0.50866$ .

In Fig. 13,  $\Delta(0)$  given by one of methods E-G always monotonically decreases, when  $m$  is increased. We know

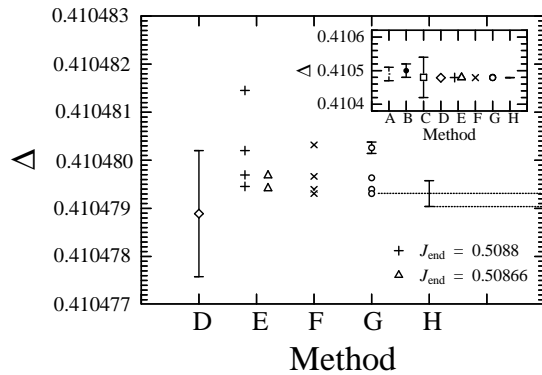


Fig. 13. The values of the Haldane Gap which have been reported and that calculated in this article. A scale of the perpendicular axis is adjusted so that all error bar are shown in the inset.

that the energy lift by the cut-off effect in the excited state is larger than that in the ground state. Besides, the systems treated in §4 have enough sizes, where any boundary effects are eliminated. Thus, we may suppose that the estimated values of  $\Delta(0)$  converge monotonically with respect to  $m \geq 120$ . Note that the difference between  $\Delta(0) = 0.41047941(1)$  when  $m = 160$  and  $\Delta(0) = 0.41047931(1)$  when  $m = 180$  is big enough compared with the fitting error.

It should be noted that the SIS estimation<sup>8</sup> gives both the lower and the upper bound for the Haldane gap. The values given by the item H provide us the best bounds with this method. When we choose  $m = 180$ , our estimations in E-G are always inside the interval given by the item H.

Thus, we may safely conclude that  $0.41047931$  should be a better upper bound of the Haldane gap than the value given by the item H. Following this discussion, we conclude that the Haldane gap is in  $[0.41047905, 0.41047931]$ . Looking at Figure 13, we may also suppose that the actual Haldane gap is closer to the upper bound than the lower bound.

For the hyperbolic deformation, the choice of  $m$  is the remaining single parameter determining the accuracy. If we consider the  $m$  dependence of the gap, we may also construct a sequence interval squeeze technique by generalizing the method given in §5. We can thus find that the use of the hyperbolic deformation is one of the efficient tool to detect the excitation gaps of one-dimensional quantum systems.

One of future subjects is numerical gap estimation of  $S = 2$  antiferromagnetic Heisenberg chain. Let us consider appropriate boundary conditions based on the valence bond solid (VBS) picture for this case. A possible simple choice is to put  $S = 1$  spins at the both ends of the system. Another simple choice is to put two  $S = 1/2$  spins at the each end of the system, where the bond configuration is the form of the letter Y. In addition, a slightly complex choice is to reduce the length of spin by amount of  $1/2$  site by site, i.e. to put  $S = 3/2, S = 1$ , and  $S = 1/2$  spins at the boundary. For each candidate of

the boundary spin arrangement, one has to consider the parametrization of the bond strength. In this way, the tuning of the boundary condition for the  $S = 2$  chain is more complicated than that of  $S = 1$  chain. Therefore, an efficient arrangement of additional boundary spins has not been reported. When the system is deformed hyperbolically, however, the problem of parameterization could be put in a extrapolation of  $\lambda$ .

Another one is to find out classical analogue of the hyperbolic deformation for 2D statistical models. A candidate is the hyperbolic lattice models studied so far,<sup>27–30</sup> but in those models only discrete values of  $\lambda$  are allowed. To construct a class of models that has appropriate structure for the DMRG applied to classical systems<sup>31</sup> would be important for the further study.

### Acknowledgements

The authors thank to Okunishi, Gendiar, and Krcmar for valuable discussions. This work was partly supported by Grants-in-Aid from the Ministry of Education, Culture, Sports, Science and Technology (MEXT) (No. 19540403 and No. 20340096), and the Global COE Program (Core Research and Engineering of Advanced Materials-Interdisciplinary Education Center for Materials Science), MEXT, Japan. A part of the computations was performed using facilities of the Information Initiative Center, Hokkaido University and the Supercomputer Center, Institute for Solid State Physics, University of Tokyo.

- 1) M.E. Fisher: in *Proc. Int. School of Physics 'Enrico Fermi'*, ed. M.S. Green, (Academic Press, New York, 1971). Vol. **51**, 1.
- 2) M.N. Barber: in *Phase Transitions and Critical Phenomena*, ed. C. Domb and J.L. Lebowitz, (Academic Press, New York, 1983), Vol. **8**, 146. and references there in.
- 3) F.D.M. Haldane: Phys. Rev. Lett. **50** (1983) 1153.
- 4) F.D.M Haldane: Phys. Lett. A **93** (1983) 464.
- 5) M.P. Nightingale and H.W.J. Blöte: Phys. Rev. B **33** (1986) 659.
- 6) H.Q. Lin: Phys. Rev. B **42** (1990) 6561.
- 7) O. Golinelli, T. Jolicœur, and R. Lacaze: Phys. Rev. B **50** (1994) 3037.
- 8) H. Nakano and A. Terai: J. Phys. Soc. Jpn. **78** (2009) 014003.
- 9) S.R. White: Phys. Rev. Lett. **69** (1992) 2863.
- 10) S.R. White: Phys. Rev. B **48** (1992) 10345.
- 11) I. Peschel, X. Wang, M. Kaulke, and K. Hallberg (Eds.): *Density-Matrix Renormalization, A New Numerical Method in Physics*, Lecture Notes in Physics (Springer, Berlin 1999).
- 12) U. Schollwöck: Rev. Mod. Phys. **77** (2005) 259.
- 13) S.R. White and D.A. Huse: Phys. Rev. B **48** (1993) 3844.
- 14) Estimation errors in numerical data obtained in this article represent the order of magnitude, rather than the deviation in strict statistical meaning.
- 15) H. Ueda and T. Nishino: J. Phys. Soc. Jpn. **78** (2009) 014001.
- 16) H. F. Trotter: Proc. Am. Math. Soc. **10** (1959) 545.
- 17) M. Suzuki: Prog. Theor. Phys. **56** (1976) 1454.
- 18) R.J. Baxter: *Exactly solved models in statistical mechanics* (Academic Press, London 1982).
- 19) The distance  $(\cosh \nu x) \Delta\tau$  diverges in the limit  $|x| \rightarrow \infty$ . This divergence can be controlled by considering finite width  $R$  and keep  $|x| < R$ .
- 20) This kind of difference cannot be neglected when one considers long-range interactions in the framework of the hyperbolic deformation.
- 21) Note that the first and the second terms in the r.h.s. of eq. (2.7) do not commute.
- 22) T. Kennedy: J. Phys. Condens. Matter **2** (1990) 5737.
- 23) P. Wynn: Numer. Math. **8** (1966) 264.
- 24) D. Shanks: J. Math. Phys. (Cambridge, Mass.) **34** (1955) 1.
- 25) O. Golinelli, T. Jolicœur, and R. Lacaze: Phys. Rev. B **50** (1994) 3037.
- 26) S. Todo and K. Kato: Phys. Rev. Lett. **87** (2001) 047203.
- 27) K. Ueda, R. Krcmar, A. Gendiar, and T. Nishino: J. Phys. Soc. Jpn. **76** (2007) 084004.
- 28) R. Krcmar, A. Gendiar, K. Ueda, and T. Nishino: J. Phys. A **41** (2008) 215001.
- 29) A. Gendiar, R. Krcmar, K. Ueda, and T. Nishino: Phys. Rev. E **77** (2008) 041123.
- 30) R. Krcmar, T. Iharagi, A. Gendiar, and T. Nishino: Phys. Rev. E **78** (2008) 061119.
- 31) T. Nishino: J. Phys. Soc. Jpn. **65** (1996) 891.